Organic/inorganic hybrid pigments from flavylium cations and palygorskite

Gustavo Thalmer M. Silva,[1] Cassio P. Silva,[1] Marcelo H. Gehlen,[2] Jessy Oake,[3] Cornelia Bohne,[3] and Frank H. Quina*,[1]

[1]Instituto de Química, Universidade de São Paulo, Av. Lineu Prestes 748, Cidade Universitária, São Paulo 05508-000, Brazil

[2]Instituto de Química de São Carlos, Universidade de São Paulo, 13566-590 São Carlos, SP, Brazil

[3]Department of Chemistry and Centre for Advanced Materials and Related Technologies (CAMTEC), University of Victoria, PO Box 1700 STN CSC, Victoria, BC, Canada, V8W 2Y2

* Corresponding author.
E-mail address: quina@usp.br

Abstract

Features such as color, brightness and fluorescence are extremely important in applications of pigments. Hybrid materials inspired by the ancient Maya Blue pigment are a promising alternative to improve the properties and applicability of natural and synthetic dyes. In this work, we report the preparation, photophysical properties, and stability of several fluorescent hybrid pigments based on flavylium cations (FL) adsorbed on palygorskite (PAL). Five flavylium cations were investigated, viz., the 3',4',7-trimethoxyflavylium (FL1), 7-hydroxy-4'-methoxy-flavylium (FL2), 7-hydroxy-4-methylflavylium (FL3), 5,7-dihydroxy-4-methylflavylium (FL4) and 7-methoxy-4-methylflavylium (FL5) cations. Only FL1 and FL2, without a methyl substituent at the 4-position that could hinder inclusion in palygorskite channels, adsorbed strongly on PAL, producing fluorescent hybrid pigments with attractive colors. The spectroscopic and fluorescence properties of the FL1/PAL and FL2/PAL hybrid pigments were characterized. The color of the adsorbed dyes was somewhat more resistant to changes in external pH, photochemical stability was maintained and the thermal lability was markedly improved in the FL/PAL hybrid pigments, pointing to flavylium cations as promising chromophores for the development of fluorescent hybrid pigments with attractive colors.

Keywords: fluorescent hybrid pigments; palygorskite; dyes; clays; flavylium cations; color.

Graphical Abstract

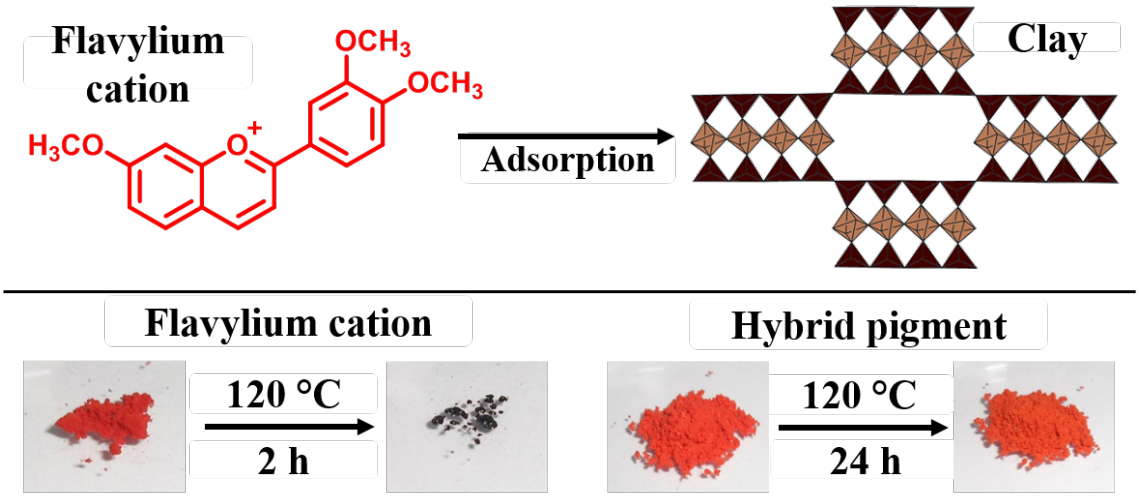

1. Introduction

Hybrid materials prepared by the combination of dyes with inorganic substrates have been extensively studied in search of materials with unique properties and color attributes (preferably bright and/or fluorescent) that are chemically, thermally and light stable (Laguna et al., 2007; Teixeira-Neto et al., 2009, 2012; Dejoie et al., 2010; Giustetto et al., 2014; Lin et al., 2014). One of the oldest and perhaps the most famous example of an organic-inorganic hybrid material is the Maya Blue pigment, which was widely used in murals, codices, ceramics and sculptures by the Maya civilization in the Pre-Columbian era. Maya Blue is extremely stable, able to resist the attack of concentrated nitric acid, bases and organic solvents without losing its color (Sánchez Del Río and Martinetto, 2006; Arnold and Branden, 2008; Chiari et al., 2008; Giustetto et al., 2011). The amazing chemical and photochemical stability of Maya Blue is presumably due to its unique structure, which consists of the dye indigo protectively (and apparently irreversibly) inserted into the channels of palygorskite or sepiolite clay (Giustetto et al., 2005, 2006, 2011; Chiari et al., 2008; Tilocca and Fois, 2009).

Palygorskite (PAL) is a hydrated magnesium and aluminum phyllosilicate clay mineral. Unlike most clays, PAL has fibrous morphology, consisting of a layer structure of ribbons of tetrahedral silica and central magnesium octahedra oriented along the fibers. The octahedral sheet is sandwiched between two tetrahedral sheets that have periodic inversion of the apical oxygen, resulting in well-defined one-dimensional cavities or tunnels (Sánchez Del Río et al., 2009; Doménech et al., 2011) with dimensions 3.7 x 6.4 Å (Brigatti et al., 2006) and, on the external surface of the clay fibers, partially open grooves or channels (as denominated for sepiolite by, e.g., Ruiz-Hitzky (2001) and Martínez-Martínez et al. (2011)). Several studies have shown that palygorskite has two

main types of acidic sites, a sites of stronger acidity with an effective pK_a in the range of 5-5.5 and more weakly acidic sites with a pK_a around 9-9.5 (Frini-Srasra and Srasra, 2008; Acebal and Vico, 2017). The porous structure of this clay allows the insertion and/or adsorption of organic molecules and ions, making it a good adsorbent (Giustetto et al., 2014; Mu and Wang, 2016). Recent studies involving dyes and PAL clay have obtained several novel Maya Blue-like pigments (Lima et al., 2012; Fan et al., 2014; Zhang et al., 2015a, 2015b; Zhang et al., 2015c, 2015d), some of which are materials with interesting self-cleaning properties (Zhang et al., 2016a, 2016b). Adsorption of dyes onto PAL and PAL composites (Mu and Wang, 2016) and biomedical applications clay-drug hybrid materials (Kim et al., 2016) have been recently reviewed and the use of PAL as an adsorbent for environmental remediation continues to be of interest (Ugochukwu et al., 2013; Boudriche et al., 2015; Yang et al, 2018).

The chromophoric group of anthocyanins, which are responsible for most of the purple, blue and red colors of flowers and fruits, is a 7-hydroxyflavylium cation. The chemical and photochemical reactivity of synthetic flavylium cations mimics that of natural anthocyanins, with the advantage of the facility and versatility of modifying the substituents on the flavylium chromophore and consequently their reactivity. Although anthocyanins and synthetic flavylium cations have great potential for practical applications as dyes or antioxidants, these applications are limited by their chemical reactivity, which is affected by several factors including pH, temperature, light, oxygen, among others (Ferreira da Silva et al., 2005; Castañeda-Ovando et al., 2009; Quina et al., 2009; Cavalcanti et al., 2011; Silva et al., 2016).

The inclusion and/or adsorption of anthocyanins and flavylium cations in/on inorganic substrates such as mesoporous materials (Kohno et al., 2008a, 2011, 2015; Gago et al., 2017) and clays (Lima et al., 2007; Kohno et al., 2007, 2009, 2010; Ogawa

et al., 2017; Ribeiro et al., 2018), may represent promising alternatives for preventing the undesirable chemistry of these dye molecules. In the present work, we have investigated the preparation of flavylium cation/palygorskite (FL/PAL) complexes as prototypes for fluorescent hybrid anthocyanin/palygorskite pigments. The complexes that retained the more intense colors and fluorescence after exhaustive washing with acidic methanol were chosen for evaluation of the thermal, photochemical and pH stability of their color and fluorescence.

2. Experimental Section

2.1. Materials

The flavylium cation salts 3',4',7-trimethoxyflavylium chloride (FL1), 7-hydroxy-4'-methoxy-flavylium chloride (FL2), 7-hydroxy-4-methylflavylium chloride (FL3), 5,7-dihydroxy-4-methylflavylium chloride (FL4) and 7-methoxy-4-methylflavylium chloride (FL5) used in this work (Scheme 1) were available from previous studies of the group and the syntheses have been previously reported (Freitas et al., 2013; Held et al., 2016; Silva et al., 2018). The palygorskite used in this work was the Source Clay PFl-1 from the Clay Minerals Society. The chemical composition, characterization and properties of this clay have been described (Shariatmadari et al., 1999; Borden and Giese, 2001; Chipera and Bish, 2001; Guggenheim and Koster van Groos, 2001; Madejová and Komadel, 2001; Mermut and Cano, 2001; Li et al., 2003; Dogan et al., 2006; Frost et al., 2010). Hydrochloric acid (HCl, Vetec) was used as received, methanol (Merck) was treated with sodium and ultrapure water was used for the preparation of all aqueous solutions.

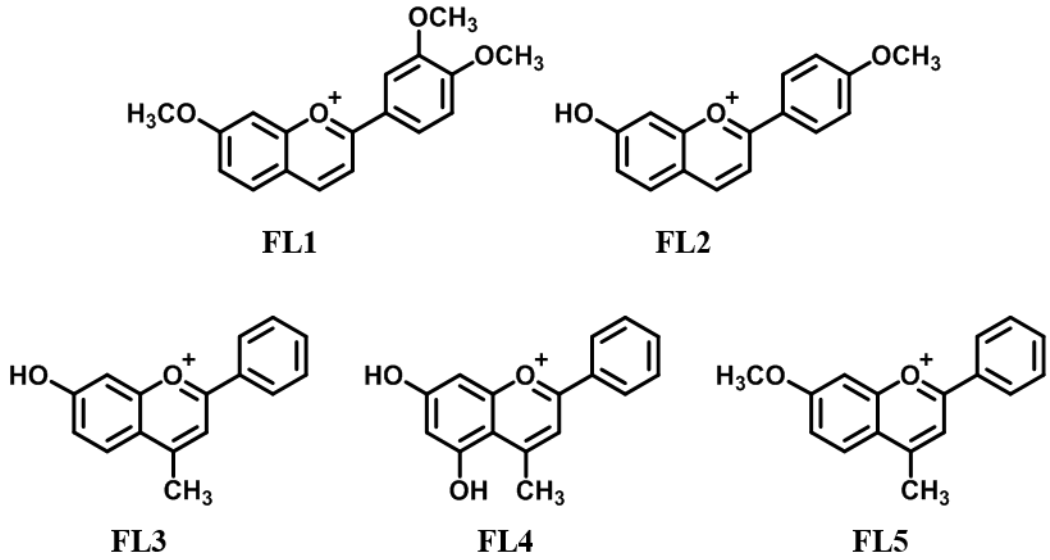

Scheme 1. Structures of the flavylium cations (FL) used in this work.

2.2. Preparation and physical characterization of the FL/PAL Hybrid Pigments

Aliquots of solutions of the FL in methanol (in which FL cations are highly soluble) containing 1% 1.0 mol dm^{-3} HCl (in order to suppress proton transfer and hydration of the flavylium cations) were added to the appropriate amount of PAL clay powder. The initial FL/PAL ratios utilized were 0.050, 0.075, 0.100 and 0.125 mmol g^{-1}. The resulting dispersions were stirred for 24 h in the dark at room temperature, centrifuged and the solid washed exhaustively with HCl-acidified methanol and dried at 45 °C under vacuum for 2 h. The amount of flavylium cation adsorbed was estimated from the decrease in the absorbance of the supernatant employing the known molar attenuation coefficient of each FL.

Powder X-ray diffractograms of PAL and FL1/PAL were determined with a Bruker D2 Phase diffractometer using Cu-K_α radiation (1.5418 Å, 30 kV, 15 mA) employing a scan step of 0.05°. Nitrogen adsorption/desorption isotherms were determined at -196 °C using a Quantachrome volumetric adsorption analyzer (Model 100E). The samples were outgassed for 24 h under reduced pressure at 80 °C. The specific

148 surface areas (S_{BET}) and total pore volumes (V_{tot}) of the samples were determined by the
149 BET (Brunauer et al., 1938) and BJH (Barrett et al., 1951) methods, respectively. Surface
150 areas of the micropores (S_{micro}), the external surface areas (S_{ext}),the micropore volumes
151 (V_{micro}) and the sum of meso- and macropore volumes ($V_{meso+macro}$) were estimated by the
152 *t*-plot method (Lippens and de Boer, 1965).

153

154 **2.3. Spectroscopic measurements**

155 For the infrared measurements, about 1.50 mg of solid sample was added to
156 approximately 150 mg of dry KBr in a small agate mortar and mixed by grinding. The
157 resulting powder was pressed into a pellet using a hydraulic press (Caver, model 3912,
158 Wabash). Infrared spectra of the pellets were collected using a Bruker Vector 22 FTIR
159 spectrophotometer in the frequency range of 4000-500 cm^{-1}, 32 scans at 0.5 cm^{-1} digital
160 resolution.

161 The UV-Vis-diffuse reflectance (DR) spectra were measured with a Varian Cary
162 50 UV-vis Bio spectrophotometer equipped with a *Barrelino*™ diffuse reflectance probe
163 (Harrick Scientific Products, Inc.). Samples with greater amounts of adsorbed flavylium
164 (FL1 and FL2) were diluted in barium sulfate. The diffuse reflectance spectra were
165 converted to the corresponding reemission function, F(R), employing the Kubelka-Munk
166 equation (Tomasini et al., 2009):

167 $$F(R) = \frac{(1-R)^2}{2R}$$

168 where R is the measured reflectance at each wavelength. CIELAB Color coordinates (CIE
169 L*a*b*) (Gilchrist and Nobbs, 1999) were obtained from the UV-vis-DR measurements
170 by using the software Agilent Cary WinUV Color. In this case, the samples were not
171 diluted in barium sulfate in order to obtain the true color coordinates of the samples.

Absorbance spectra were measured using the same spectrophotometer or a Hewlett Packard 8452A diode array spectrometer.

All steady state fluorescence measurements were performed with a Hitachi F-4500 fluorescence spectrophotometer. For analysis of the solid samples, the instrument was equipped with a solid sample holder. The excitation and emission wavelengths are indicated in the figure legends. The slits were set to bandwidths of 5.0 nm for both excitation and emission monochromators of the hybrid pigments, and for FL1 and FL2 were 10/20 and 2.5/5.0 nm (excitation and emission), respectively. The experiments with the hybrid pigments were conducted in the solid state. For the steady-state fluorescence anisotropy measurements, the fluorescence spectrophotometer (Hitachi F-4500) was fitted with manual polarizers placed in the excitation and emission light pathways. The steady-state anisotropy (r) was calculated for the emission intensities determined for the four orientations of the polarizers: vertical-vertical (VV), vertical-horizontal (VH), horizontal-horizontal (HH) and horizontal-vertical (HV) employing the following equation (Lakowicz, 2006):

$$r = \frac{I_{\mathrm{VV}} - G I_{\mathrm{VH}}}{I_{\mathrm{VV}} + 2G I_{\mathrm{VH}}}$$

where $G = I_{HV}/I_{HH}$ is a correction factor for the relative sensitivity of the detection system to horizontally and vertically polarized light.

Time-resolved fluorescence decay experiments were carried out using an OB920 single photon counting system (Edinburgh Instruments), exciting the sample with a 405 nm Picosecond Pulsed Diode Laser (EPL405). The solid sample was placed in a shallow quartz cell that was covered with a quartz glass and was placed in a front-face sample holder which is tilted so as to minimize specular reflections (Zhang et al., 2014). The bandwidth for the emission monochromator was 16 nm. A neutral density filter was employed for control of the photon flux from the excitation source that reached the

197 sample. The emission wavelengths set for the collection of the decays for the FL1/PAL
198 and FL2/PAL samples were 575 and 525 nm, respectively. The fluorescence decays were
199 collected with a 50 ns time window and the number of counts in the channel with
200 maximum intensity was 10,000. Barium sulfate powder was used as a scatterer to collect
201 the instrument response function (IRF). The fluorescence decays were fit to a sum of
202 exponentials employing Edinburgh Instruments F900 software for reconvolution to
203 extract the lifetimes. The quality of the fits was determined by the randomness of the
204 residuals and the χ^2 values, which are ideally between 0.9 and 1.3.

205 For the anisotropy experiments, the diode laser was rotated to achieve vertical and
206 horizontal polarizations of the excitation beam. For the emission collection, the polarizer
207 between the sample and the emission monochromator was set to the required angles. The
208 anisotropy decay measurements were performed with a 20 ns time window and the time
209 required to collect 10000 counts was estimated. This time and the neutral density setting
210 for the excitation beam were kept constant for the collection of the 4 decays with the
211 different polarizations. The four decays were collected for each anisotropy calculation
212 (I_{VV}, I_{VH}, I_{HV}, I_{HH}) and combined to obtain the anisotropy decay (Lakowicz, 2006):

213 $$r(t) = \frac{I_{VV}(t) - GI_{VH}(t)}{I_{VV}(t) + 2GI_{VH}(t)}$$

214 The anisotropy decay, calculated using the F900 software, was then fit to a sum of
215 exponentials to estimate rotational correlation lifetimes.

216

217 **2.4. Wide Field and Confocal Fluorescence Microscopy**

218 Confocal fluorescence images were obtained using a plate scanning instrument
219 based on a microscope (Olympus IX71) with a digital piezoelectric controller and stage
220 (PI, E-710.3CD and P-517.3CD) for nanometric sample scanning. The excitation of the
221 samples at 473 nm was provided by a Cobolt Blue diode laser. The circularly polarized

222 laser beam was focused on the samples with an UPLFLN 40X Olympus objective. The
223 emission signal was separated from the laser excitation beam using Chroma Z470rd and
224 ZET 473NF dichroic and notch filter, respectively. Photons were counted using an
225 avalanche photodiode point detector (Perkin Elmer, SPCM-AQR-14) aligned with a 50
226 μm pinhole in the confocal line. Transistor-transistor logic (TTL) detector signals were
227 registered in a counter/timer PCI card (NI 6601) and transferred to a personal computer
228 for 2D plotting using a scanning control program written in C# (Ferreira et al., 2011).
229 Fluorescence images were recorded using false-color mapping, reaching the best contrast
230 enhancement according to the difference in intensity of the fluorescence signal. Wide-
231 field images were obtained with the same fluorescence microscope by adapting an optical
232 lens in the epifluorescence entrance with focus on the back aperture of the objective. The
233 samples were excited at 405 nm with a Coherent Cube CW laser and the emission was
234 selected by a dichroic cube (Chroma, z405lp) and images were registered in a color
235 camera (ThorLabs DCU223C) coupled to the right primary port of the Olympus IX71
236 (Lauer et al., 2014).
237
238 **2.5. Photochemical and Thermal stability and sensitivity to pH**
239 The UV radiation resistance tests of the samples were performed using an Oriel®
240 (California, USA) Sol UV-2 Solar simulator (85.7 % UV-A, 11 % UV-B and 3.3 % of
241 visible light). The samples were exposed to a radiation intensity of 75.0 W m^{-2} UV-A
242 (365 nm) and 43.0 W m^{-2} UV-B (312 nm). The irradiations were carried out at room
243 temperature (25 °C) with an exposure time of 6 h. UV-vis-DR measurements were used
244 to verify any spectral and color changes.
245 In order to verify the reactivity of the FL cations adsorbed into/onto PAL,
246 FL1/PAL and FL2/PAL samples were added to 5 mL of 10 mmol dm^{-3} phosphate buffer

247 solution at pH = 9. After 24 h, the samples were centrifuged and dried. UV-vis-DR
248 measurements were used to verify any spectral and color changes. In order to compare
249 the stability of the hybrid pigments with the respective free FL, the spectra of FL in 10
250 mmol dm^{-3} phosphate buffer solution, pH = 8.5, were also obtained. The reversibility was
251 examined by adding FL to 10 mmol dm^{-3} acetate buffer solutions at pH = 4, 5 or 6,
252 followed by addition of 0.1 g of PAL after discoloration of the solutions due to hydration
253 of the flavylium cation. This test was carried out under stirring at room temperature (ca.
254 20 ºC) and accomplished by taking digital images as a function of the time.

255 Thermal stability was investigated by submitting FL1/PAL and FL2/PAL samples
256 to heating at 120 °C under vacuum for 24 h and comparing with FL cations in solid form
257 that were submitted to the same temperature for 2 h. Measurements of the color
258 coordinates and digital images were used to verify any color changes.

259

260 3. Results and discussion

261 3.1. Hybrid Pigment Formation

262 Initial studies clearly showed that the relative amount of flavylium cation
263 adsorbed and the colors of the samples were influenced by the substituents on the FL
264 cations. Five FL cations with similar substituents at different positions but with different
265 pH-dependent equilibria and different molecular sizes and solvophobicity/solvophilicity,
266 were chosen for evaluation. Both FL1 and FL2 adsorbed strongly on PAL (Table 1) and
267 imparted attractive colors to the samples (Figure S1 of the Supplementary Material), even
268 after exhaustive washing with acidic methanol with the objective of removing loosely
269 physiosorbed dye. In contrast, the other three flavylium cations all have a methyl group
270 at the 4-position, i.e., FL3, FL4 and FL5, and all adsorbed poorly on PAL, failing to
271 impart attractive coloration to the clay. In the case of FL4, the amount adsorbed was

272 miniscule, as shown in Table 1 and in Figure S2 of the Supplementary Material. Since
273 affinity and stability should parallel each other, our subsequent studies of the hybrid
274 pigments focused on those derived from FL1 and FL2, i.e., FL1/PAL and FL2/PAL,
275 respectively.

276

277 **Table 1.** Relative amounts of flavylium cation adsorbed, in μmol per g of PAL.

Initial FL/PAL ratio	***FL1***	***FL2***	***FL3***	***FL4***	***FL5***
50	40	24	12	< 0.1	< 1
75	59	29	7	< 0.1	9
100	67	31	19	< 0.1	3
125	72	33	12	< 0.1	14

278

279 **3.2. X-Ray Diffraction and N_2 adsorption isotherms**

280 The powder X-ray diffractograms of FL1/PAL with the highest dye loading were
281 indistinguishable from that of the raw PAL clay itself (Figure S3 of the Supplementary
282 Material), which was in turn the same as that published for the raw PFl-1 Source Clay
283 (Chipera and Bish, 2001). This is an expected result since the dye loading was nonetheless
284 still relatively low and the interlayer spacings of one-dimensional clays such as
285 palygorskite are known to be fairly insensitive to the inclusion of organic molecules
286 (Giustetto et al., 2014; Chang et al., 2016; Yang et al., 2018).

287 Table 2 shows the specific surface areas (S_{BET}) and total pore volumes (V_{tot}) of
288 the FL1/PAL and FL2/PAL samples with the highest amounts of adsorbed dyed (72 and
289 33 μmol g^{-1}, respectively) and of a PAL reference sample exhaustively washed with
290 methanol containing 1% 1.0 mol dm^{-3} HCl determined from N_2 adsorption isotherms by
291 the BET (Brunauer et al., 1938) and BJH (Barrett et al., 1951) methods, respectively.
292 Table 2 also indicates the surface areas of the micropores (S_{micro}), the external surface
293 areas (S_{ext}), the micropore volumes (V_{micro}) and the sum of meso- and macropore volumes

($V_{meso+macro}$) estimated by the *t*-plot method (Lippens and de Boer, 1965). For FL1/PAL, the reduction in surface area was primarily due to the decrease in the external area S_{ext}, while FL2/PAL exhibited decreases in both the external and micropore surface areas and in the accessible pore volumes.

Table 2: Surface areas and pore volumes of acid-washed PAL, FL1/PAL = 72 and FL2/PAL = 33.

Sample	S_{BET} / m^2g^{-1}	S_{micro} / m^2g^{-1}	S_{ext} / m^2g^{-1}	V_{micro} / cm^3g^{-1}	$V_{meso+macro}$ / cm^3g^{-1}	V_{tot} / cm^3g^{-1}
PAL[a]	137	21	116	0.011	0.475	0.486
FL1/PAL	126	22	104	0.011	0.462	0.473
FL2/PAL	126	15	111	0.008	0.420	0.428

[a] after washing with HCl-acidified methanol.

3.3. Spectroscopic and Photophysical Studies

FTIR spectra of PAL clay and of the FL1 and FL2 derived hybrid pigments were recorded in the region from 4000 cm^{-1} to 500 cm^{-1} (Figure S4 of the Supplementary Material). The raw clay exhibits absorption bands in the range 3000-3600 cm^{-1}, along with a band at 1654 cm^{-1}, corresponding respectively to the stretching and bending vibrations of water molecules (coordinated and zeolitic) (Frost et al., 2010; Giustetto and Wahyudi, 2011; Fan et al., 2014; Zhang et al., 2015b; Zhang et al., 2015c, 2015d). The region 3000-3600 cm^{-1} also includes contributions from the OH-stretching vibrations of Mg/Al-OH groups (Frost et al., 2010; Zhang et al., 2015a; Zhang et al., 2015d). The band at 3615 cm^{-1} corresponds to Al-OH stretching (Frost et al., 2010; Zhang et al., 2015b; Zhang et al., 2015d) and/or Si-OH stretching (Giustetto and Wahyudi, 2011). Bands in the range from 975 to 1196 cm^{-1} are attributed to Si-O vibrations (Frost et al., 2010; Zhang

315 et al., 2015b; Zhang et al., 2015c) and the weak band at 797 cm^{-1} is characteristic of quartz
316 impurities (Frost et al., 2010; Zhang et al., 2015b). In the infrared spectra of the FL/PAL
317 samples, additional bands characteristic of FL cations were detected in the range of 1200-
318 1600 cm^{-1} (Figure 1). In particular, the absorption bands at 1356 cm^{-1} and 1352 cm^{-1} for
319 FL1/PAL and FL2/PAL samples, respectively, correspond to C-O-C stretching. The
320 intensities of the FL bands are quite weak because of the relatively small amount of
321 flavylium cation in relation to clay and exhibit hypsochromic shifts compared to the FL
322 cation salts, reflecting the interactions between FL and PAL.

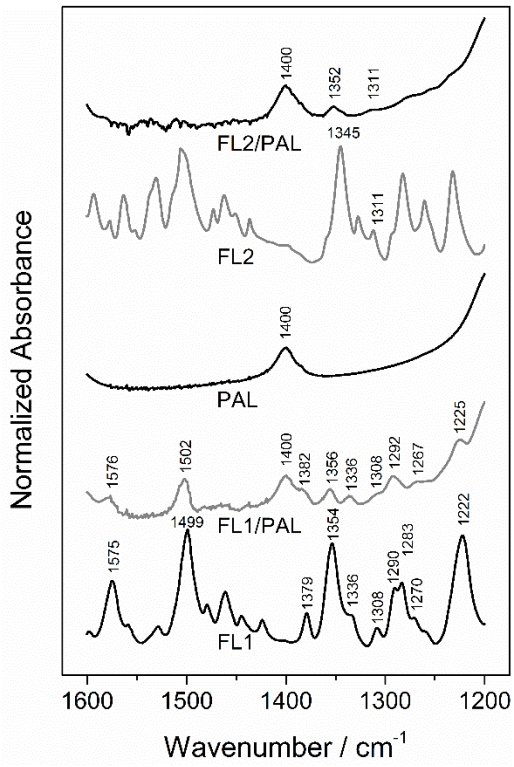

323

324 **Figure 1.** Infrared spectra of PAL, FL1, FL2, FL1/PAL (72 μmol) and FL2/PAL (33
325 μmol) in the range 1200-1600 cm^{-1}. Note: The broad peak at 1400 cm^{-1} is an
326 impurity in the KBr used.

327

328 UV-vis absorption spectra of FL1 and FL2 in 1% 1.0 mol dm^{-3} HCl/methanol
329 solution present absorption maxima at 478 and 465 nm, respectively (Figures 2a and 2b).
330 The UV-vis-DR spectra of the hybrid pigments in the same Figures exhibit a small red

shift from 478 nm to around 492 nm for FL1, and 465 nm to 470 nm for FL2. Spectral shifts of this type have been attributed to the effect of electrostatic interactions between organic molecules and the inorganic substrate (Kohno et al., 2008a, 2009) or to the acidity of the inorganic substrate (Kohno et al., 2008b). Although aggregates are relatively common for the adsorption of dyes on clays (Valandro et al., 2015, 2017), the spectra did not present any evidence of the presence of FL aggregates, indicating that the washing step as part of the adsorption procedure efficiently removed excess FL cations that might participate in aggregate formation.

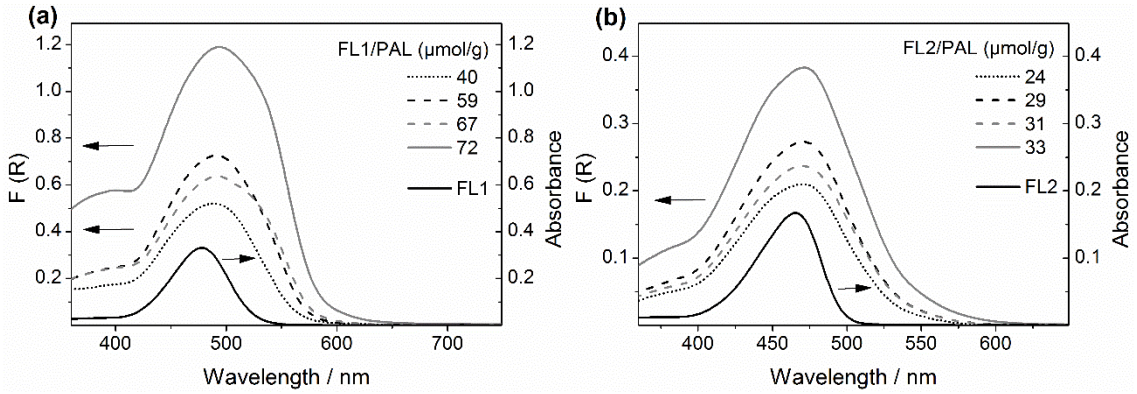

Figure 2. UV-vis and UV-vis-DR spectra (Kubelka-Munk mode) of (a) FL1 and FL1/PAL, and (b) FL2 and FL2/PAL samples.

Figure 3 shows the fluorescence excitation and emission spectra of the hybrid pigments FL1/PAL and FL2/PAL, together with those of FL1 and FL2 in 1% 1.0 mol dm^{-3} HCl/methanol solution. In 1% 1.0 mol dm^{-3} HCl/methanol solution, FL1 presented a broad fluorescence emission band with a maximum around 577 nm and FL2 a maximum at 509 nm. The corresponding fluorescence excitation spectra resemble the absorption spectra, with maxima at 487 and 468 nm for FL1 and FL2, respectively. The two hybrid pigments showed emission in the same region as the corresponding FL in solution. For FL2/PAL, the maximum fluorescence emission was at ca. 525 nm and did not shift significantly with increasing amount of adsorbed FL. For FL1/PAL, however, the

fluorescence emission maximum underwent a red-shift from 577 to 600 nm with increasing amount of adsorbed FL1. In the case of Auramine O adsorbed on SYn-1 and SAz-1 clays, a decrease in intensity and shift to longer wavelengths of the fluorescence emission with increasing dye adsorption was attributed to H-aggregate formation (Valandro et al., 2015). However, FL/PAL hybrid pigments exhibited no additional absorption bands of the type expected for J- or H-aggregates, suggesting that the apparent shift with increasing adsorbed FL1 is more likely a distortion of the emission spectrum due to reabsorption, i.e., to an inner filter effect. For both solid hybrid pigments, the front-face geometry emission intensity decreased as the amount of adsorbed flavylium cation increased (Figure 3), suggesting self-quenching.

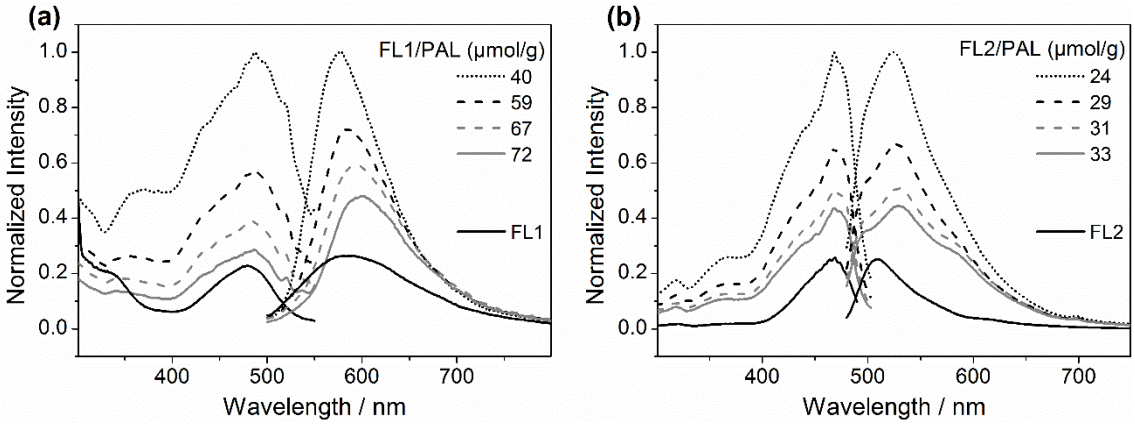

Figure 3. Excitation and emission spectra of (a) FL1 (Ex. 480 and Em. 576 nm) in 1% 1.0 mol dm^{-3} HCl/methanol solution and solid FL1/PAL (Ex. 470 and Em. 576 nm; adsorbed amounts of FL1 are indicated in μmol/g); (b) FL2 (Ex. 467 and Em. 508 nm) in 1% 1.0 mol dm^{-3} HCl/methanol solution and solid FL2/PAL (Ex. 467 and Em. 525 nm; adsorbed amounts of FL1 are indicated in μmol/g) samples.

Time-resolved emission measurements (405 nm excitation; 575 nm emission for FL1/PAL and 525 nm emission for FL2/PAL) indicated fast biexponential decay with

lifetimes (± 15%) of FL1/PAL (0.35 and 1.0 ns with normalized preexponentials of ca. 0.8 and 0.2, respectively) about half those of FL2/PAL (0.6 and 2.0 ns with normalized preexponentials of ca. 0.6 and 0.4, respectively). Steady-state fluorescence anisotropies (r) ranged from 0.03-0.05 for FL1/PAL and 0.06-0.07 for FL2/PAL, apparently insensitive to the amount of adsorbed FL. Time-resolved anisotropy measurements showed an extremely fast initial depolarization, within ca. ≤ 100 ps, with a residual anisotropy at long times consistent with that found in the steady-state measurements. This suggests that fast intermolecular energy transfer or migration between FL molecules is the main mechanism responsible for the rapid loss of anisotropy and could also contribute to the decrease in fluorescence intensity with increasing amount of adsorbed flavylium cation.

Wide field fluorescence images (Figure S5 of the Supplementary Material; true color) indicate a homogeneous distribution of adsorbed FL without differentiating between adsorption inside or on the edges of the channels, with the difference in intensities due largely to differences in the focal planes. In agreement with the red shift of the emission seen in the fluorescence spectra, the fluorescence color of the FL1/PAL particles changes with the amount of FL1 adsorbed, as can be seen in Figure S5 of the Supplementary Material. Images recorded by confocal fluorescence microscopy using false-color mapping are shown in Figure S6 of the Supplementary Material. Although these images indicate that the particles are not homogeneous in size or shape, all are strongly fluorescent, with the highest intensities in the regions of the focal plane around the particle core. Unfortunately, the dye loadings were much too high to make single-molecule measurements on isolated particles or fibers (Martínez-Martínez et al., 2011).

3.3. Stability Tests of the Hybrid Pigments

Resistance of the adsorbed dye to extraction with organic solvent and acid is, in essence, intrinsic to the method of preparation of the hybrid pigments. Thus, the flavylium dissolved in acidic methanol were allowed to adsorb by contact with the clay and the resultant materials then washed exhaustively with acidic methanol to remove any readily extractable dye. Although the dyes are also highly soluble in water, water did not extract the dye from either FL1/PAL or FL2/PAL.

The photochemical stability of flavylium cations is usually much better than their thermal stability. Indeed, both the solid pigments and the hybrid pigments showed good photostability, with the color being essentially unaltered by irradiation for 6 h in a solar UV simulator. Thus, adsorption of the dyes onto the clay does not markedly reduce their photostability. On the other hand, there was substantial improvement in the thermal stability of both FL1 and FL2 adsorbed on palygorskite, as has been reported for flavylium cations adsorbed on other types of clay (Kohno et al., 2007, 2010) or protonated zeolites (Kohno et al., 2008a). A temperature of 120 ^{o}C. was chosen for the thermal stability tests since temperatures up to 120-150 ^{o}C have been used for the thermal analysis sepiolite/indigo and PAL/indigo hybrid materials (Hubbard et al., 2003) and, in the case of PAL (Guggenheim and Koster van Gross, 2001), this temperature is just above the range where most of the weakly adsorbed water has been lost and where the more strongly adsorbed water only begins to be lost. Thus, while both FL1 and FL2 degraded substantially in less than 2 h at this temperature in a vacuum oven, both hybrid pigments largely retained their characteristic colors (Table 3 and Figures S7-S9 and Tables S1 and S2 of the Supplementary Material) after 24 h under these conditions.

Table 3. CIELAB color coordinates for the hybrid pigments before and after heating at 120 ^{o}C. for 24 h.

Samples		L*	a*	b*
FL1/PAL = 72	Before heating	55.8438	50.5605	58.3429
FL1/PAL = 72	After 24 h at 120 °C.	51.1756	43.4934	52.4811
FL2/PAL = 33	Before heating	73.6264	17.4510	79.0872
FL2/PAL = 33	After 24 h at 120 °C.	60.3541	28.2977	56.6914

In aqueous solution, both FL1 and FL2 undergo hydration above about pH 3 to form the hemiacetal (B), followed by ring-opening tautomerization to form the *cis*-chalcone (ZC) and then slow isomerization to the *trans*-chalcone (EC) (Held et al., 2016). The 7-hydroxy group of FL2 can also deprotonate at slightly higher pH, resulting in the conjugate base (A); the corresponding equilibria are shown for FL2 in Scheme S1 of the Supplementary Material. Spectra of FL1 or FL2 registered after 1 h in pH = 8.5 phosphate buffer solution and of the hybrid pigments after immersion for 24 h in pH = 9 phosphate buffer solution are shown in Figure 4. For FL1 a new band appeared around 380 nm corresponding to a mixture of B, ZC and EC, while FL2 presented two new bands, one at around 490 nm assigned to a conjugate base formed by deprotonation of the hydroxyl group of one or more of the species resulting from the hydration-induced equilibria. The spectra of FL1/PAL and FL2/PAL also showed two bands at longer wavelength, one in the region of the adsorbed cation and the other in the same regions as FL1 and FL2 in solution at similar alkaline pH.

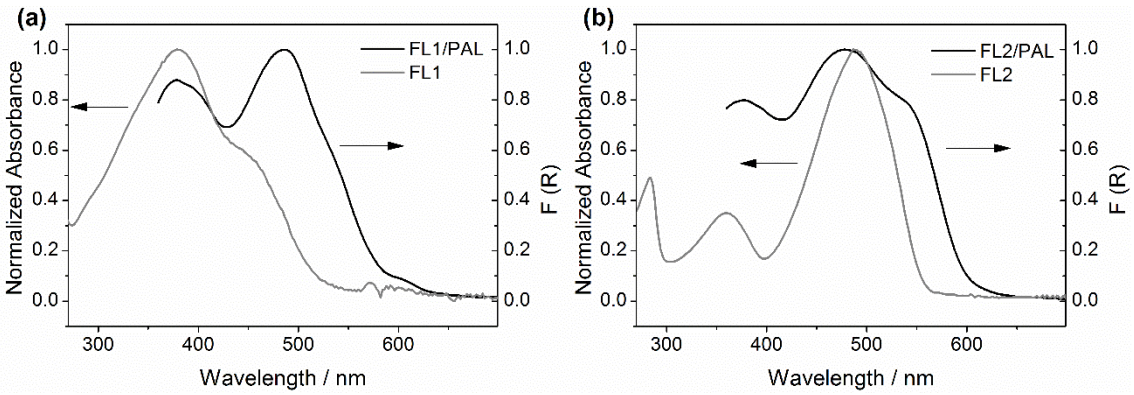

Figure 4. Absorbance and diffuse reflectance spectra (Kubelka-Munk mode) for (a) FL1 and FL1/PAL and (b) FL2 and FL2/PAL. The absorbance spectra were collected for FL1 and FL2 incubated for 1 h in pH 8.5 solution, and the UV-vis-DR spectra were collected after FL1/PAL and FL2/PAL were immersed for 24 h in pH 9 solution, centrifuged and dried.

Figure S10 of the Supplementary Material illustrates the impact of the basic aqueous medium on the color of the hybrid pigments before and after immersion at pH 9 and Table S3 of the Supplementary Material shows the CIELAB color coordinate data. Although the color of FL1/PAL became less intense upon immersion in pH 9 aqueous solution, it still showed an attractive color compared to FL1 at the same pH, indicating that the adsorption process made it less prone to hydration. However, FL2/PAL changed color completely, indicating that the adsorption process did not prevent deprotonation of a significant fraction of the adsorbed FL2 molecules. In both cases, the dye did not leach from the clay and the color changes were reversible upon acidification of the medium, indicating chemical stability under these conditions.

3.5 The dye-clay interaction

Since flavylium cations are highly soluble in methanol, the exhaustive washing with acidic methanol should remove any excess or weakly physiosorbed dye, leaving only strongly bound dye. This points to ion exchange as potentially the most important mode

460 of interaction of these cationic dyes with palygorskite. In this regard, the final amounts
461 of the flavylium cations adsorbed (Table 1) were all well below the cation exchange
462 capacity (CEC) values reported for the PFl-1 Source Clay palygorskite utilized in this
463 work: 175 (Borden and Giese, 2001) and 165 (Li et al., 2003) and, after a partial
464 purification, 140 μmol g^{-1} (Shariatmadari et a., 1999). Nonetheless, because all five of
465 the initially tested dyes are cationic, ion exchange alone cannot explain the marked
466 differences in affinity for the clay. Thus, the presence of a methyl group at the 4 position
467 of the flavylium chromophore of FL3 and FL5 substantially reduced the net adsorption
468 and, in the case of FL4, the presence of an additional hydroxyl group at position 5 of the
469 chromophore completely eliminated its adsorption after washing (Table 1). Indeed, as
470 shown in Figure 5 (See Figure S11 in the Supplementary Material for a color version),
471 the additional methyl group makes these compounds too wide to insert into the tunnels or
472 external grooves of PAL. However, the two compounds without the 4-methyl group could
473 insert partially, though not totally into the tunnels and/or interact with the open grooves
474 on the external surface. Because FL2 is slightly smaller than FL1, it should fit into the
475 tunnels somewhat better than FL1. This is consistent with the surface area and pore
476 volume measurements (Table 2), which suggest a preference of FL1 for the external
477 grooves and of FL2 for both external grooves and partial insertion into tunnels.
478
479
480
481
482

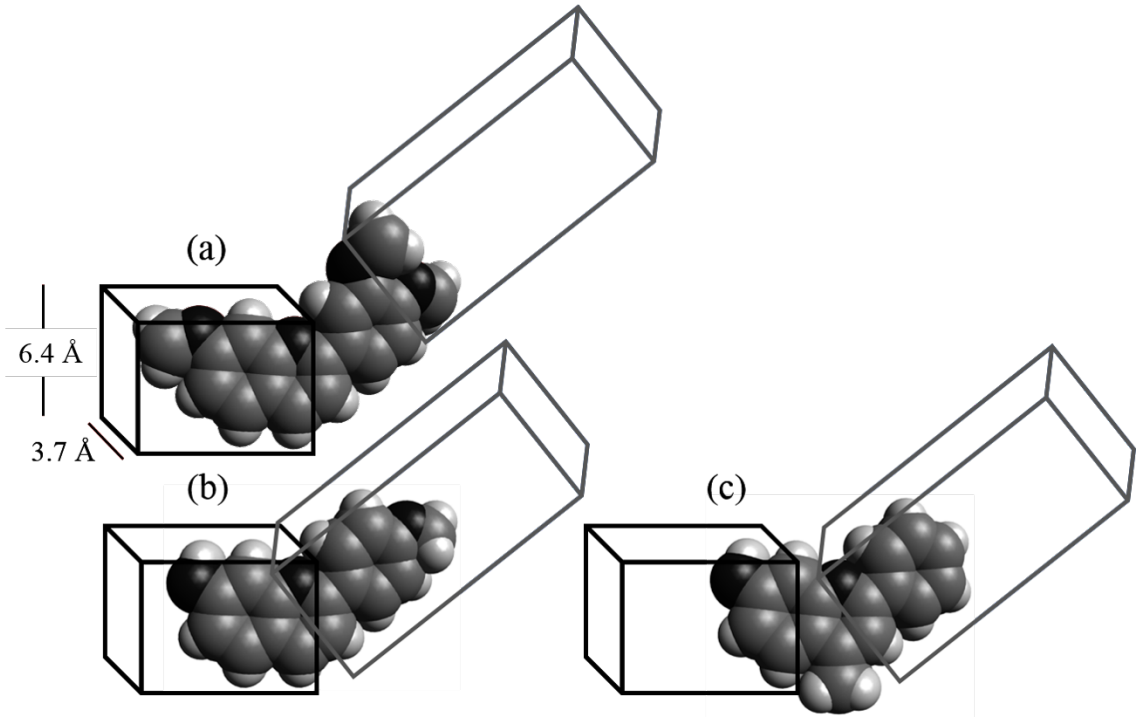

Figure 5. Comparison of the molecular sizes of (a) FL1, (b) FL2 and (c) FL3 with the dimensions of the tunnels of palygorskite (Brigatti et al., 2006).

Several studies have shown that the cationic form of anthocyanins and flavylium ions can be selectively stabilized aqueous solution by incorporating them into anionic micelles (Lima et al., 2002; Quina et al., 2009) or by inclusion in supramolecular complexes (Held et al., 2016). Because the apparent hydration constant of FL1 (pK_h, or the pH at which half of the cation form is hydrated) is 3.0 ± 0.3 (Held et al., 2016), solutions of FL1 in acetate buffer at pH 4, 5 or 6 are nearly colorless (Figures S12-S14 of the Supplementary Material), reflecting the almost complete conversion of the flavylium cation form of FL1 to the hydrated species. Upon addition of PAL to these solutions, the suspended clay gradually acquired the red color of the adsorbed FL1 cation as a function of time, indicating the conversion of the hydrated forms in solution to the adsorbed cationic form on the clay. If only the cationic form adsorbed from solution onto the clay, there should be a clear difference in the apparent rates of adsorption at these three distinct

pH values due to the large pH-dependent differences in the equilibrium concentration of this form. However, the rates of appearance of the coloration were qualitatively very similar at pH 4 and pH 5, but clearly much faster than at pH 6. Likewise, the maximum intensity of the color at long times (2 weeks) was similar for the two lower pH values, and much more intense than at pH 6 (Figures S12-S14 of the Supplementary Material). Indeed, this strongly suggests that it is the hydrated forms that adsorb on PAL under these conditions and that they are subsequently converted to the cationic form by interaction with the more highly acidic sites of the clay with effective pK_a around pH 5-5.5 (*vide supra*).

4. Conclusions

Simple electrostatic interactions are incompatible with the observed differences in adsorption of FL cations on PAL. The adsorption was particularly inefficient for FL cations bearing a 4-methyl group, consistent with steric inhibition of interaction with the palygorskite tunnels or external grooves as the major contributor to differences in adsorption. Adsorption on PAL stabilized the cationic form of the flavylium cations FL1 and FL2 against hydration to at least pH 5, apparently reflecting the participation of the more highly acidic sites on the PAL surface. The photochemical stability was retained and the chemical and thermal stabilities of the cation form of FL1 and FL2 were substantially improved by adsorption on PAL, pointing to flavylium cations of this type as promising chromophores for the development of novel fluorescent hybrid pigments with attractive colors.

Acknowledgements

The authors thank the CNPq (F.H.Q. Universal grant 408181/2016-3), INCT-Catálise, and NAP-PhotoTech for the support, the CNPq for a research productivity fellowships (F.H.Q. and M.H.G.), and CAPES for graduate fellowships (G.T.M.S. and C.P.S.). Researchers at UVic thanks NSERC (RGPIN-2017-04458) for funding and CAMTEC for the use of shared facilities. The authors thank Josué M. Gonçalves for assistance in determining the X-ray diffractograms and Dr. Thiago Lewis Reis Hewer, Dept. of Chemical Engineering, Polytechnic School, USP, for performing the N_2 sorption measurements.

References

Acebal, S.G., Vico, L.I., 2017. Acid-Base Properties of Aqueous Suspensions of Homoionic Sepiolite and Palygorskite. Nat. Resour. 8, 432–444. https://doi.org/10.4236/nr.2017.86028

Arnold, E., Branden, J., 2008. The first direct evidence for the production of Maya Blue: rediscovery of a technology. Antiquity 82, 151–164. https://doi.org/10.1017/S0003598X00096514

Barrett, E. P., Joyner, L. G., Halenda, P. P. 1951. The Determination of Pore Volume and Area Distributions in Porous Substances. I. Computations from Nitrogen Isotherms. J. Am. Chem. Soc. 73, 373-380. https://doi.org/10.1021/ja01145a126

Borden, D., Giese, R. F. 2001. Baseline studies of the Clay Minerals Society source clays: Cation exchange capacity measurements by the ammonia-electrode method. Clays Clay Miner. 49, 444-445. https://doi.org/10.1346/CCMN.2001.0490510

Boudriche, L., Calvet, R., Chamayou, A., Hamdi, B., Balard, H., 2015. Removal of lead(II) from aqueous solution using modified palygorskite, contribution of inverse

549 gas chromatography. J. Chromatogr. A 1408, 207-216.
550 https://doi.org/10.1016/j.chroma.2015.07.011
551 Brigatti, M.F., Galan, E., Theng, B.K.G., 2006. Structures and Mineralogy of Clay
552 Minerals, in: Chapter 2, Handbook of Clay Science, Developments in Clay Science.
553 pp. 19–86. https://doi.org/10.1016/S1572-4352(05)01002-0
554 Brunauer, S., Emmett, P. H., Teller, E., 1938. Adsorption of Gases in Multimolecular
555 Layers**.** J. Am. Chem. Soc. 60, 309-319. https://doi.org/10.1021/ja01269a023
556 Castañeda-Ovando, A., Pacheco-Hernández, M. de L., Páez-Hernández, M.E.,
557 Rodríguez, J.A., Galán-Vidal, C.A., 2009. Chemical studies of anthocyanins: A
558 review. Food Chem. 113, 859–871. https://doi.org/10.1016/j.foodchem.2008.09.001
559 Cavalcanti, R.N., Santos, D.T., Meireles, M.A.A., 2011. Non-thermal stabilization
560 mechanisms of anthocyanins in model and food systems-An overview. Food Res.
561 Int. 44, 499–509. https://doi.org/10.1016/j.foodres.2010.12.007
562 Chang, P.-H., Jiang, W.-T., Li, Z., Kuo, C.-Y., Wu, Q., Jean, J. S., Lv, G. 2016.
563 Interaction of ciprofloxacin and probe compounds with palygorskite PFL-1. J.
564 Hazard. Mater. 303, 55-63. https://doi.org/10.1016/j.hazmat.2015.10.012
565 Chiari, G., Giustetto, R., Druzik, J., Doehne, E., Ricchiardi, G., 2008. Pre-columbian
566 nanotechnology: Reconciling the mysteries of the maya blue pigment. Appl. Phys.
567 A Mater. Sci. Process. 90, 3–7. https://doi.org/10.1007/s00339-007-4287-z
568 Chipera, S. J., Bish, D. L. 2001. Baseline studies of the Clay Minerals Society Source
569 Clays: Powder X-ray diffraction analysis. Clays Clay Miner. 49, 398-409.
570 Dejoie, C., Martinetto, P., Dooryhée, E., Strobel, P., Blanc, S., Bordat, P., Brown, R.,
571 Porcher, F., Sanchez Del Rio, M., Anne, M., 2010. Indigo@silicalite: A new
572 organic-inorganic hybrid pigment. ACS Appl. Mater. Interfaces 2, 2308–2316.
573 https://doi.org/10.1021/am100349b

574 Dogan, A. U., Dogan, M., Onal, M., Sarikaya, Aburub, A., Wurster, D. E. 2006. Baseline
575 studies of the Clay Minerals Society Source Clays: Specific surface area by the
576 Brunauer Emmett Teller (BET) method. Clays Clay Miner. 54, 62-66.
577 Doménech, A., Doménech-Carbó, M.T., Edwards, H.G.M., 2011. On the interpretation
578 of the Raman spectra of Maya Blue: A review on the literature data. J. Raman
579 Spectrosc. 42, 86–96. https://doi.org/10.1002/jrs.2642
580 Fan, L., Zhang, Y., Zhang, J., Wang, A., 2014. Facile preparation of stable
581 palygorskite/cationic red X-GRL@SiO $_2$ “Maya Red” pigments. RSC Adv. 4,
582 63485–63493. https://doi.org/10.1039/C4RA13739F
583 Ferreira da Silva, P., Lima, J. C., Freitas, A. A., Shimizu, K., Maçanita, A. L., Quina, F.
584 H., 2005. Charge-transfer complexation as a general phenomenon in the
585 copigmentation of anthocyanins. J. Phys. Chem. A 109, 7329–7338.
586 https://doi.org/10.1021/jp052106s
587 Ferreira, A. P. G., Frederice, R., Janssen, K. P. F., Gehlen, M. H., 2011. Dually
588 fluorescent silica nanoparticles. J. Lumin. 131, 888–893.
589 https://doi.org/10.1016/j.jlumin.2010.12.019
590 Freitas, A. A, Maçanita, A. A. L., Quina, F.H., 2013. Improved analysis of excited state
591 proton transfer kinetics by the combination of standard and convolution methods.
592 Photochem. Photobiol. Sci. 12, 902–10. https://doi.org/10.1039/c3pp25445c
593 Frini-Srasra, N., Srasra, E., 2008. Determination of Acid-Base Properties of HCl Acid
594 Activated Palygorskite by Potentiometric Titration. Surf. Eng. Appl. Electrochem.
595 44, 401–409. https://doi.org/10.3103/S1068375508050116
596 Frost, R.L., Xi, Y., He, H., 2010. Synthesis, characterization of palygorskite supported
597 zero-valent iron and its application for methylene blue adsorption. J. Colloid
598 Interface Sci. 341, 153–161. https://doi.org/10.1016/j.jcis.2009.09.027

599 Gago, S., Pessêgo, M., Laia, C.A.T., Parola, A.J., 2017. pH-Tunable Fluorescence and
600 Photochromism of a Flavylium-Based MCM-41 Pigment. ACS Omega 2, 122–126.
601 https://doi.org/10.1021/acsomega.6b00381
602 Gilchrist, A., Nobbs, J. 1999. Colorimetry, Theory. In Encyclopedia of Spectroscopy and
603 Spectrometry, Second Ed. (2010), J. Lindon, G. Tranter, D. Koppenaal, Eds. -
604 Academic Press, NY; pp. 380-385.
605 Giustetto, R., Wahyudi, O., 2011. Sorption of red dyes on palygorskite: Synthesis and
606 stability of red/purple Mayan nanocomposites. Microporous Mesoporous Mater.
607 142, 221–235. https://doi.org/10.1016/j.micromeso.2010.12.004
608 Giustetto, R., Llabrés I Xamena, F.X., Ricchiardi, G., Bordiga, S., Damin, A., Gobetto,
609 R., Chierotti, M.R., 2005. Maya blue: A computational and spectroscopic study. J.
610 Phys. Chem. B 109, 19360–19368. https://doi.org/10.1021/jp048587h
611 Giustetto, R., Levy, D., Wahyudi, O., Chiari, G., 2006. Crystal structure refinement of
612 Maya Blue pigment prepared with deuterated indigo, using neutron powder
613 diffraction. Eur. J. Mineral. 18, 629–640. https://doi.org/10.1127/0935-
614 1221/2006/0018-0629
615 Giustetto, R., Levy, D., Wahyudi, O., Ricchiardi, G., Vitillo, J.G., 2011. Crystal structure
616 refinement of a sepiolite/indigo Maya Blue pigment using molecular modelling and
617 synchrotron diffraction. Eur. J. Mineral. 23, 449–466. https://doi.org/10.1127/0935-
618 1221/2011/0023-2105
619 Giustetto, R., Vitillo, J.G., Corazzari, I., Turci, F., 2014. Evolution and reversibility of
620 host/guest interactions with temperature changes in a methyl red@palygorskite
621 polyfunctional hybrid nanocomposite. J. Phys. Chem. C 118, 19322–19337.
622 https://doi.org/10.1021/jp4091238
623 Guggenheim, S., Koster van Groos, A. F. 2001. Baseline studies of the Clay Minerals

624 Society Source Clays: Thermal Analysis. Clays Clay Miner. 49, 433-443.
625 https://doi.org/10.1346/CCMN.2001.0490507
626 Held, B., Tang, H., Natarajan, P., da Silva, C.P., Silva, V. O., Bohne, C., Quina, F.H.,
627 2016. Cucurbit[7]uril inclusion complexation as a supramolecular strategy for color
628 stabilization of anthocyanin model compounds. Photochem. Photobiol. Sci. 15, 752–
629 757. https://doi.org/10.1039/C6PP00060F
630 Hubbard, B., Kuang, W., Moser, A., Facey, G. A., Detellier, C. 2003. Structural study of
631 Maya blue: textural, thermal and solid state multinuclear magnetic resonance
632 characterization of the palygorskite-indigo and sepiolite-indigo adducts. Clays Clay
633 Miner. 51, 318-326.
634 Kim, M. H., Choi, G., Elzatahry, A., Vinu, A. Choy, Y. B., Choy, J.-H., 2016. Review of
635 clay-drug hybrid materials for biomedical applications: administration routes. Clays
636 Clay Miner. 64, 115-130. https://doi.org/10.1346/CCMN.2016.0640204
637 Kohno, Y., Hoshino, R., Matsushima, R., Tomita, Y., Kobayashi, K., 2007. Stabilization
638 of Flavylium Dyes by Incorporation in the Clay Interlayer. J. Jpn. Soc. Colour Mater.
639 80, 6–12. https://doi.org/https://doi.org/10.4011/shikizai1937.80.6
640 Kohno, Y., Shibata, Y., Oyaizu, N., Yoda, K., Shibata, M., Matsushima, R., 2008a.
641 Stabilization of flavylium dye by incorporation into the pore of protonated zeolites.
642 Microporous Mesoporous Mater. 114, 373–379.
643 https://doi.org/10.1016/j.micromeso.2008.01.023
644 Kohno, Y., Tsubota, S., Shibata, Y., Nozawa, K., Yoda, K., Shibata, M., Matsushima, R.,
645 2008b. Enhancement of the photostability of flavylium dye adsorbed on mesoporous
646 silicate. Microporous Mesoporous Mater. 116, 70–76.
647 https://doi.org/10.1016/j.micromeso.2008.03.014
648 Kohno, Y., Kinoshita, R., Ikoma, S., Yoda, K., Shibata, M., Matsushima, R., Tomita, Y.,

649 Maeda, Y., Kobayashi, K., 2009. Stabilization of natural anthocyanin by
650 intercalation into montmorillonite. Appl. Clay Sci. 42, 519–523.
651 https://doi.org/10.1016/j.clay.2008.06.012
652 Kohno, Y., Hoshino, R., Ikoma, S., Shibata, M., Matsushima, R., Tomita, Y., Maeda, Y.,
653 Kobayashi, K., 2010. Stabilization of Flavylium Dye by Incorporation into Bentonite
654 Clay. J. Jpn. Soc. Colour Mater. 83, 103–107.
655 https://doi.org/https://doi.org/10.4011/shikizai.83.103
656 Kohno, Y., Senga, M., Shibata, M., Yoda, K., Matsushima, R., Tomita, Y., Maeda, Y.,
657 Kobayashi, K., 2011. Stabilization of flavylium dye by incorporation into Fe-
658 containing mesoporous silicate. Microporous Mesoporous Mater. 141, 77–80.
659 https://doi.org/10.1016/j.micromeso.2010.11.004
660 Kohno, Y., Kato, Y., Shibata, M., Fukuhara, C., Maeda, Y., Tomita, Y., Kobayashi, K.,
661 2015. Enhanced stability of natural anthocyanin incorporated in Fe-containing
662 mesoporous silica. Microporous Mesoporous Mater. 203, 232–237.
663 https://doi.org/10.1016/j.micromeso.2014.10.042
664 Laguna, H., Loera, S., Ibarra, I.A., Lima, E., Vera, M.A., Lara, V., 2007. Azoic dyes
665 hosted on hydrotalcite-like compounds: Non-toxic hybrid pigments. Microporous
666 Mesoporous Mater. 98, 234–241. https://doi.org/10.1016/j.micromeso.2006.09.009
667 Lakowicz, J. R. 2006. Principles of Fluorescence Spectroscopy, 3rd edition, Springer,
668 New York; pp. 353-412.
669 Lauer, M.H., Gehlen, M.H., De Jesus, K., Berlinck, R.G.S., 2014. Fluorescence
670 spectroscopy and confocal microscopy of the mycotoxin citrinin in condensed phase
671 and hydrogel films. J. Fluoresc. 24, 745–750. https://doi.org/10.1007/s10895-013-
672 1347-y
673 Li, Z., Willms, C. A., Kniola, K. 2003. Removal of anionic contaminants using surfactant-

674 modified palygorskite and sepiolite. Clays Clay Miner., 51, 445-451.
675 Lima E, Martinez-Ortiz MJ, Fregoso E, Mendez-Vivar J. 2007. Capturing natural
676 chromophores on natural and synthetic aluminosilicates. Stud. Surf. Sci. Catal. 170,
677 2110-2115. https://doi.org/10.1016/S0167-2991(07)81107-4
678 Lima, E., Guzmán, A., Vera, M., Rivera, J.L., Fraissard, J., 2012. Aged natural and
679 synthetic Maya Blue-like pigments: What difference does it make? J. Phys. Chem.
680 C 116, 4556–4563. https://doi.org/10.1021/jp207602m
681 Lima, J. C., Vautier-Giongo, C., Lopes, A., Melo, E., Quina, F. H., Maçanita, A. L. 2002.
682 Color Stabilization of Anthocyanins: Effect of SDS Micelles on the Acid−Base and
683 Hydration Kinetics of Malvidin 3-Glucoside (Oenin). J Phys. Chem. A, 106, 5851-
684 5859. https://doi.org/10.1021/jp014081c
685 Lin, Y.H., Hori, Y., Hoshino, S., Miyazawa, C., Kohno, Y., Shibata, M., 2014.
686 Fluorescent colored material made of clay mineral and phycoerythrin pigment
687 derived from seaweed. Dye. Pigment. 100, 97–103.
688 https://doi.org/10.1016/j.dyepig.2013.08.022
689 Lippens, B. C., de Boer, J. H. 1965. Studies on pore systems in catalysts: V. The *t* method.
690 J. Catal. 4, 319-323. https://doi.org/10.1016/0021-9517(65)90307-6
691 Madejová, J., Komadel, P. 2001. Baseline studies of the Clay Minerals Society Source
692 Clays: Infrared methods. Clays Clay Miner. 49, 410-432.
693 Martínez-Martínez, V., Corcóstegui, C., Prieto, J. B., Gartzia, L., Sallares, S., Arbeloa, I.
694 L. 2011. Distribution and orientation study of dyes intercalated into single sepiolite
695 fibers. A confocal fluorescence microscopy approach. J. Mater. Chem. 21, 269-276.
696 https://doi.org/10.1039/c0jm02211j
697 Mermut, A.R., Cano, A. F. 2001. Baseline studies of the Clay Minerals Society Source
698 Clays: Chemical analyses of major elements. Clays Clay Miner. 49, 381-386.

699 Mu, B., Wang, A., 2016. Adsorption of dyes onto palygorskite and its composites: A
700 review. J. Environ. Chem. Eng. 4, 1274–1294.
701 https://doi.org/10.1016/j.jece.2016.01.036
702 Ogawa, M., Takee, R., Okabe, Y., Seki, Y. 2017. Bio-geo hybrid pigment; clay-
703 anthocyanin complex which changes color depending on the atmosphere. Dyes
704 Pigments, 139, 561-565. https://doi.org/10.1016/j.dyepig.2016.12.054
705 Quina, F.H., Moreira, P.F., Vautier-Giongo, C., Rettori, D., Rodrigues, R.F., Freitas,
706 A.A., Silva, P.F., Macanita, A.L., 2009. Photochemistry of anthocyanins and their
707 biological role in plant tissues. Pure Appl. Chem. 81, 1687–1694.
708 https://doi.org/10.1351/Pac-Con-08-09-28
709 Ribeiro, H. L., Oliveira, A. V. D., Brito, E. S. D., Ribeiro, P. R. V., Souza Filho, M. D.
710 S. M., Azeredo, H. M. C. 2018, Stabilizing effect of montmorillonite on acerola juice
711 anthocyanins. Food Chem, 245, 966-973.
712 https://doi.org/10.1016/j.foodchem.2017.11.076
713 Ruiz-Hitzky, E. 2001. Molecular access to the intracrytalline tunnels of sepiolite. J.
714 Mater. Chem. 11, 86-91. https://doi.org/10.1039/b003197f
715 Sánchez Del Río, M., Martinetto, P., 2006. Synthesis and Acid Resistance of Maya Blue
716 Pigment. Archaeometry 48, 115–130. https://doi.org/10.1111/j.1475-
717 4754.2006.00246.x
718 Sánchez Del Río, M., Boccaleri, E., Milanesio, M., Croce, G., Van Beek, W., Tsiantos,
719 C., Chyssikos, G.D., Gionis, V., Kacandes, G.H., Suárez, M., García-Romero, E.,
720 2009. A combined synchrotron powder diffraction and vibrational study of the
721 thermal treatment of palygorskite-indigo to produce Maya blue. J. Mater. Sci. 44,
722 5524–5536. https://doi.org/10.1007/s10853-009-3772-5
723 Shariatmadari, H., Mermut, A. R., Benke, M. B. 1999. Sorption of selected cationic and

724 neutral organic molecules on palygorskite and sepiolite. Clays Clay Miner. 47, 44-
725 53.
726 Silva, V.O., Freitas, A.A., Maçanita, A.L., Quina, F.H., 2016. Chemistry and
727 photochemistry of natural plant pigments: the anthocyanins. J. Phys. Org. Chem. 29,
728 594–599. https://doi.org/10.1002/poc.3534
729 Silva, C. P., Pioli, R. M., Liu, L., Zheng, S., Zhang, M., Silva, G. T. de M., Carneiro, V.
730 M. T., Quina, F. H., 2018. Improved Synthesis of Analogues of Red Wine
731 Pyranoanthocyanin Pigments. ACS Omega 3, 954–960.
732 https://doi.org/10.1021/acsomega.7b01955
733 Teixeira-Neto, Â.A., Shiguihara, A.L., Izumi, C.M.S., Bizeto, M.A., Leroux, F.,
734 Temperini, M.L.A., Constantino, V.R.L., 2009. A hybrid material assembled by
735 anthocyanins from açaí fruit intercalated between niobium lamellar oxide. Dalt.
736 Trans. 4136–4145. https://doi.org/10.1039/b820610d
737 Teixeira-Neto, Â.A., Izumi, C.M.S., Temperini, M.L.A., Ferreira, A.M.D.C.,
738 Constantino, V.R.L., 2012. Hybrid Materials Based on Smectite Clays and
739 Nutraceutical Anthocyanins from the Açaí Fruit. Eur. J. Inorg. Chem. 2012, 5411–
740 5420. https://doi.org/10.1002/ejic.201200702
741 Tilocca, A., Fois, E., 2009. The color and stability of maya blue: TDDFT calculations. J.
742 Phys. Chem. C 113, 8683–8687. https://doi.org/10.1021/jp810945a
743 Tomasini, E.P., Román, E.S., Braslavsky, S.E., 2009. Validation of fluorescence quantum
744 yields for light-scattering powdered samples by laser-induced optoacoustic
745 spectroscopy. Langmuir 25, 5861–5868. https://doi.org/10.1021/la803492k
746 Ugochukwu, U. C., Jones, M. D., Head, I. M., Manning, D. A. C., Fialips, C. I. 2014.
747 Biodegradation of crude oil saturated fraction supported on clays. Biodegradation
748 25, 153-165. https://doi.org/10.1007/s10532-013-9647-0

749 Valandro, S.R., Poli, A.L., Neumann, M.G., Schmitt, C.C., 2015. Photophysics of
750 auramine O adsorbed on solid clays. J. Lumin. 161, 209–213.
751 https://doi.org/10.1016/j.jlumin.2015.01.023
752 Valandro, S.R., Poli, A.L., Correia, T.F.A., Lombardo, P.C., Schmitt, C.C., 2017.
753 Photophysical Behavior of Isocyanine/Clay Hybrids in the Solid State. Langmuir 33,
754 891–899. https://doi.org/10.1021/acs.langmuir.6b03898
755 Yang, R., Li, D., Li, A., Yang, H. 2018. Adsorption properties and mechanisms of
756 palygorskite for remocal of various ionic dyes from water. Appl. Clay Sci. 151, 20-
757 28. https://doi.org/10.1016/j.clay.2017.10.016
758 Zhang, H.T., Li, R., Yang, Z., Yin, C.-X., Gray, M.R., Bohne, C., 2014. Evaluating
759 steady-state and time-resolved fluorescence as a tool to study the behavior of
760 asphaltene in toluene. Photochem. Photobiol. Sci. 13, 917–928.
761 https://doi.org/10.1039/c4pp00069b
762 Zhang, Y., Wang, W., Mu, B., Wang, Q., Wang, A., 2015a. Effect of grinding time on
763 fabricating a stable methylene blue/palygorskite hybrid nanocomposite. Powder
764 Technol. 280, 173–179. https://doi.org/10.1016/j.powtec.2015.04.046
765 Zhang, Y., Wang, W., Zhang, J., Liu, P., Wang, A., 2015b. A comparative study about
766 adsorption of natural palygorskite for methylene blue. Chem. Eng. J. 262, 390–398.
767 https://doi.org/10.1016/j.cej.2014.10.009
768 Zhang, Y., Fan, L., Chen, H., Zhang, J., Zhang, Y., Wang, A., 2015c. Learning from
769 ancient Maya: Preparation of stable palygorskite/methylene blue@SiO2 Maya Blue-
770 like pigment. Microporous Mesoporous Mater. 211, 124–133.
771 https://doi.org/10.1016/j.micromeso.2015.03.002
772 Zhang, Y., Zhang, J., Wang, A., 2015d. Facile preparation of stable palygorskite/methyl
773 violet@SiO2 “Maya Violet” pigment. J. Colloid Interface Sci. 457, 254–263.

https://doi.org/10.1016/j.jcis.2015.07.030

Zhang, Y., Dong, J., Sun, H., Yu, B., Zhu, Z., Zhang, J., Wang, A., 2016a. Solvatochromic Coatings with Self-Cleaning Property from Palygorskite@Polysiloxane/Crystal Violet Lactone. ACS Appl. Mater. Interfaces 8, 27346–27352. https://doi.org/10.1021/acsami.6b09252

Zhang, Y., Zhang, J., Wang, A., 2016b. From Maya blue to biomimetic pigments: durable biomimetic pigments with self-cleaning property. J. Mater. Chem. A 4, 901–907. https://doi.org/10.1039/C5TA09300G